Vehicle Experiment of Low Frequency UWB Bistatic SAR with Ground-Based Receiver

Hongtu Xie[1, 2, 3, 4], Shaoying Shi[3], Junfa Mao[1], Daoxiang An[4], and Fuhai Li[2]
[1] Key Laboratory of Ministry of Education of Design and Electromagnetic Compatibility of High Speed Electronic Systems, Shanghai Jiao Tong University (SJTU), Shanghai, China
[2] College of Electrical and Information Engineering, Hunan University, Changsha, China
[3] Air Force Early Warning Academy, Wuhan, China
[4] College of Electronic Science, National University of Defense Technology (NUDT), Changsha, China
Email: xht20041623@163.com, {xiehongtu08, daoxiangan}@nudt.edu.cn, jfmao@sjtu.edu.cn, xht20041623@sina.com

***Abstract*— Low Frequency Ultrawideband Bistatic Synthetic Aperture Radar (LF UWB BSAR) can produce the higher resolution image and obtain the added information of scenes. In the paper, a vehicle experiment of the LF UWB BSAR is described and the result is proposed. This BSAR system has a LF UWB SAR system as the vehicle-based transmitter and the other LF UWB radar system as a ground-based receiver. In August 2015, the vehicle experiment was conducted in Changsha in China, and the LF UWB BSAR raw data was collected. The aim was to investigate the imaging property of the LF UWB BSAR system. 1-PPS signal in combination with the Global Position System (GPS) disciplined 100MHz oscillator from GPS receivers were used to implement the time/frequency synchronization of LF UWB BSAR systems. Bistatic image was obtained using the subaperture spectrum equilibrium method integrated with the Fast Factorized Back Projection (FFBP) algorithm. Excellent results prove the validity of the vehicle experiment of the LF UWB BSAR.**

***Index Terms*—bistatic synthetic aperture radar, ground-based receiver, low frequency ultrawideband, experiment**

I. Introduction

Recent years, many remote sensing and geoscience applications are developed on the synthetic aperture radar (SAR) [1]-[6]. Bistatic SAR (BSAR) systems were built by several countries in both military and civilian fields, and some well experiment results were obtained [7]-[9].

Compared with the monostatic SAR, the BSAR has the complex configurations because it can be designed and deployed flexibly to satisfy the different applications [10]. For the same scene, BSAR has the greater anti-jamming ability than the monostatic case. If BSAR system includes more than one receivers or transmitters, the imaging scene can be illuminated at different angles, which can acquire the added information of scenes. One-stationary BSAR (OS-BSAR) is an azimuth variant BSAR system [11], [12], which has a moving transmitter or receiver and a stationary receiver or transmitter fixed at a high position. OS-BSAR not only inherits the advantages of the general BSAR, but also is easy to implement imaging, thus it has attracted the much attention.

Manuscript received June 10, 2017; revised November 29, 2017.

Low Frequency Ultrawideband (LF UWB) SAR system operates in the LF UWB signal with a large fractional bandwidth and the wide antenna beamwidth associated with a large integration angle, so it can provide the higher resolution SAR image [13]-[15]. Hence, it is a significant advantage that the OS-BSAR operates in LF UWB modes. Some countries conducted LF UWB BSAR experiments, and several results were obtained [9], [16], [17].

However, the LF UWB OS-BSAR experiment poses various challenges, such as the synchronization between transmitter and receiver, position measurement of radars, polarimetric calibration, collection geometry planning, and data processing. Most important challenge is the successful operation of the LF UWB OS-BSAR. To test the imaging property of the LF UWB OS-BSAR system, we conducted a programme of upgrades to add a bistatic collection ability to the monostatic LF UWB SAR system.

The paper presents a developed LF UWB OS-BSAR system with the vehicle-based transmitter and ground-based receiver, experimental campaign, data processing and experimental results. In Section II, the development of the LF UWB OS-BSAR system is given, focusing on the collection ability of the LF UWB OS-BSAR data. The LF UWB OS-BSAR experiment and data processing are discussed in Section III. The experimental results are presented in Section IV. Section V gives a conclusion.

II. Development of LF UWB OS-BSAR System

In 2011, a programme of the upgrades to add a bistatic collection ability to the monostatic SAR was commenced by National University of Defense Technology (NUDT), which is developed using the hardware and software of two monostatic LF UWB SAR systems operating at P band with the fractional bandwidth of about 0.25 [5]. A proof-of-concept of the LF UWB OS-BSAR experiment was performed in 2014. In August 2015, the vehicle experiment was conducted in campus in Changsha, China.

A. Transmitting and Receiving Systems

Vehicle-based LF UWB transmitting system transmits the P band chirp signal to a region in the strip map mode, and then the ground-based LF UWB receiving system illuminates the same region and receives the scattered

doi: 10.18178/ijsps.5.4.136-140

data of the scene. Fig. 1 gives the vehicle-based LF UWB transmitting system, which is integrated onboard vehicle (Fig. 1(a)) and fixed on its carriage (Fig. 1(b)). The caliber coupling multilayer patch antennas for transmitting the radar signal is fixed on the roof the vehicle. Transmitting antenna has a 3 dB azimuth beamwidth from 30° to 55° and a 3 dB elevation beamwidth from 70° to 90°, with the gain 10dB. One Pulse Per Second (1PPS) signal from the GPS receiver is transferred into the center controller to control the timing reference of this system, and then the GPS synchronization module provides the coherence frequency reference for this system, and it is used to drive a frequency synthesizer to produce various clock signals for different parts of this system. Under the control of the center controller, the wave generator generates the P band chirp signal. And then, it is modulated into the radio frequency signal, attenuated by the adjustable attenuator and amplified by the power amplifier. At last, it is transmitted by the transmitting antenna. In addition, the vehicle-based transmitting system position is got by GPS motion compensation module to offer the precise motion compensation. Fig. 2 gives the ground-based LF UWB receiving system, which is placed on the step in the west of the square, with the receiving antenna mounted on the top of a tripod (Fig. 2(a)). In Fig. 2, the receiving antenna receives the scattered data of the scene. It is transferred into the low noise amplifier, down-converted into the intermediate frequency signal, filtered and amplified by the power amplifier, and demodulated into the in-phase signal and quadrature signal. Then, the demodulated signals are sampled by the high-speed sampler, converted by the analogue-to-digital converter, and then recorded on the solid state electronic array and fed to the personal computer. Similarly, for the receiving system, the 1PPS signal from the GPS receiver is transferred into the center controller to control the timing reference of this system, and the GPS synchronization module provides the coherence frequency reference for this system, and it is used to drive a frequency synthesizer to produce various clock signals for different parts of this system.

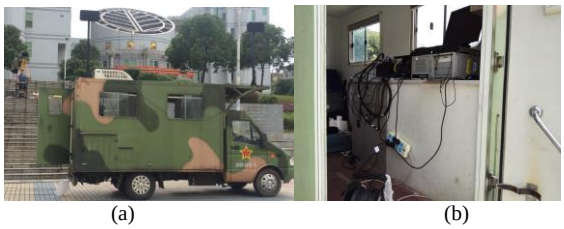

(a) (b)

Figure 1. Vehicle-based LF UWB transmitting system. (a) vehicle; (b) carriage installation viewed from outside.

(a) (b)

Figure 2. Ground-based LF UWB receiving system. (a) antenna; (b) receiving system.

B. *Time and Frequency Synchronization*

To achieve the time and frequency synchronization between vehicle-based transmitting system and ground-based receiver system, the GPS receivers have been used as the reference clock and trigger generators. 1PPS signal from the GPS receivers is an accessible common trigger useful for the bistatic requirement, which can solve the timing synchronization problem. Before the experimental campaign, we thoroughly investigated and measured the 1-PPS deviations between GPS receivers. The measured results showed that, after about 20 minutes warm up period, two independent GPS systems have a maximum drift of only 30ns between the 1-PPS signals during 15 minutes of measurements, and thus this time deviation is acceptable for our application. Based on measured results, we decided to synchronize the developed LF UWB OS-BSAR system through this common trigger.

Some GPS receivers offer a 100MHz reference clock synchronized to 1-PPS signal. Such a type of the GPS disciplined oscillator is used as the system reference clock and is a solution for the frequency synchronization issue. The Voltage-Controlled Oscillator (VCO) generates the standard sine signal. After the amplification and frequency conversion, it is transferred to a phase detector, and it is phase detected by the 1PPS signal. The phase error from the phase detector is used to discipline the VCO, and the output signal from them in turn stabilizes the VCO by the digital phase-locked loop. VCO produces the coherent reference signals in two radar systems, and then are used to drive a frequency synthesizer to produce various system signals in each system.

In conclusion, 1-PPS signal in combination with the GPS disciplined 100MHz oscillator allow the vehicle-based transmitting and ground-based receiving systems to become coherent and synchronized.

III. VEHICLE EXPERIMENT OF LF UWB OS-BSAR

A. *Vehicle Experiment*

In August 2015, the vehicle experiment of the LF UWB OS-BSAR was conducted in campus in Changsha, China. The aim of this experiment was to test the imaging property of the developed LF UWB OS-BSAR system and the validity of the data processing. Fig. 3 shows the imaging geometry and optical image of the imaging scene. In Fig. 3(a), ground-based receiving system was placed on the step in the west of the square, with the receiving antenna mounted on the roof of a tripod. Vehicle-based transmitting system was integrated onboard a vehicle, and the transmitting antenna is mounted at the roof of the vehicle. The dashed line is the ideal track of the vehicle, and the solid curve is its actual track. The vehicle-based transmitting antenna illuminates imaging scene including several targets, and the ground-based receiving antenna receives the bistatic HH polarisable scattered data.

The parameters of the LF UWB OS-BSAR system is listed in Table I. Vehicle moves along Y axis direction with the speed about 3.5m/s, and the scene scattered signal is collected from a wide variety of the azimuth

look direction. The initial positions of vehicle-based transmitting antenna is about (0, 0, 4)m at the zeros time, while the position of the ground-based receiving antenna is about (-21, 49.6, 6)m. The scene lies in a line-of-sight of the ground-based receiving antenna, and thus the constrained operation of this LF UWB OS-BSAR system to imaging scene is only a few decameter from the tripod. To collect data over a range of the incidence angles, the distance of scene center was varied: the typical distance ranged from 35 to 55m, which produces the incidence angle of the vehicle-based transmitting antenna from 80.3 ° to 80.8 °, and the incidence angle of ground-based receiving antenna from 85.91 ° to 86.9 °. Finally, one data site was selected for the data processing: scene was a flat area, and scene center was approximately 66m from the tripod. The scene size was about 50m in the X axis and 80m in the Y axis, respectively. The scene center is (45, 40, 0)m. Various targets, such as the metallic reflectors, metallic cylinders, as well as the metallic sphere and metallic mast, were deployed at the imaging scene prior to the vehicle experiment, in order to validate the imaging property of the LF UWB OS-BSAR and the scattering characteristics of the various targets. The positions of the metallic reflectors are (37.8, 38.8, 0)m, (48.2, 49.2, 0)m and (58.6, 59.6, 0)m, respectively. And, the positions of the metallic cylinders are (32.7, 46.6, 0)m, (32.7, 49.2, 0)m and (32.7, 51.8, 0)m, respectively. The position of the metallic mast is about (40, 31, 0)m.

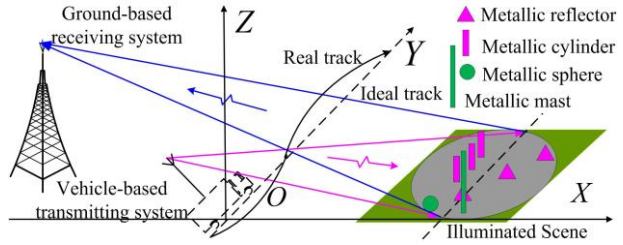

(a)

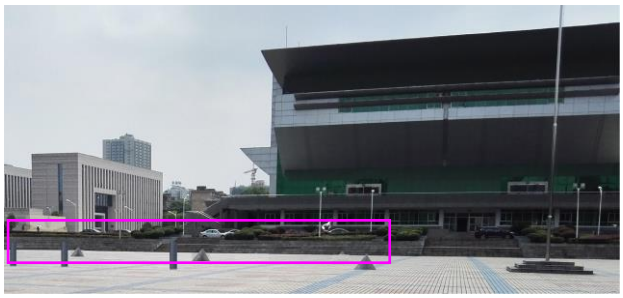

(b)

Figure 3. (a) Imaging geometry; (b) optical image of imaging scene.

TABLE I. PARAMETERS OF LF UWB OS-BSAR SYSTEM

Parameter	Value	Parameter	Value
Signal frequency	P band	Sampling frequency	220MHz
Integration angle	50 °	Pulse repetition frequency	500MHz
Pulse duration	100ns	Vehicle speed	3.5m/s
Receiving antenna position	(-21, 49.6, 6)m	Transmitting antenna initial position	(0,0,4)m

B. *Data Processing*

LF UWB OS-BSAR system operates in the P band and has the wide antenna beamwidth associated with a large wide integration angle, so there are several difficulties in the data processing, i.e., huge amount of scattered data, serious range-azimuth coupling, large and spatial-variant range cell migration, and the complex motion errors. The Fast Factorized Back Projection (FFBP) algorithm [18] and the Modified Nonlinear Chirp Scaling (MNLCS) algorithm [19] are used for the data processing of the LF UWB OS-BSAR data, which are corresponding to the time-domain algorithm and frequency-domain algorithm. And, the motion compensation method based on the GPS data and parameters estimation is used to remove the influence of the platform's motion errors. Imaging results of the data show that, compared with the MNLCS algorithm, the FFBP algorithm has better performance in the accurate imaging under the complex bistatic geometry, and could achieve the larger focused scene and the smaller image geometry distortion. Thus, in the following, the LF UWB OS-BSAR image is obtained using the FFBP algorithm.

Besides, there is a strong Radio Frequency Interference (RFI) saturated by the ground-based receiving system working in the P band. The influence of RFI signals may be extremely significant since their power is much higher than the reflected power of the LF UWB OS-BSAR. To remove its influence, a subaperture spectrum equilibrium method [20] integrated with a FFBP method is used in the data processing. In addition, there may be a time error of the scattered data caused by the uncertain time delay in the LF UWB OS-BSAR system, which can be corrected using the direct waveform from the vehicle-based transmitting antenna to ground-based receiving antenna.

Finally, before the RFI suppression is performed, the data of the LF UWB OS-BSAR (including the GPS data) should be preprocessed. First, the GPS data should be upsampled and filtered, and then transferred into the Cartesian coordinate system to obtain the local position of the vehicle-based antenna. Then, the scattered data of the illuminated scene should be downsampled and filtered.

IV. EXPERIMENTAL RESULTS

Fig. 4 gives the bistatic scattered data of the scene in the time-domain and frequency-domain. Form Fig. 4(a), the real (blue line) and imaginary components (red line) of the bistatic scattered data is very complicated due to the complicated bistatic geometry. Besides, it can be seen that the scattered data of targets in the frequency domain, since the targets are deployed at the flat and open square, their scattered data is very strong.

Fig. 5 shows the LF UWB OS-BSAR image obtained by the FFBP method, which is shown that the scene is well focused. Besides, it can be seen only a small part of the bistatic image appears well illuminated. Because the ground-based receiving antenna results in the narrow antenna footprint, which may produce the rapid roll-off of brightness towards the lateral edges of the bistatic image. First, it is seen that the focused quality of the metallic reflectors in the red rectangle will become bad compared

with the monostatic case, due to the lower resolution of the LF UWB OS-BSAR system. Besides, the relative scattered power of the metallic cylinder (as well as the metallic mast) in the yellow ellipse will become strong compared with the monostatic case, due to the isotropic scattering of the metallic cylinder. Finally, we find that only a metallic sphere in the white circle in Fig. 5 is seen. The reason is that some targets in the white circle aren't illuminated by the ground-based receiving antenna.

In order to quantitatively evaluate the focusing quality of the LF UWB OS-BSAR image in Fig. 5, the amplitude profiles of the imaging result of one metallic reflector in the X and Y axes are extracted from Fig. 5. Moreover, the resolutions of the selected focused metallic reflector in the X and Y axes are measured based on the width of the amplitude profiles at -3dB. The measured resolutions of the selected metallic reflector in the X and Y axes are 1.71m and 0.33m, respectively.

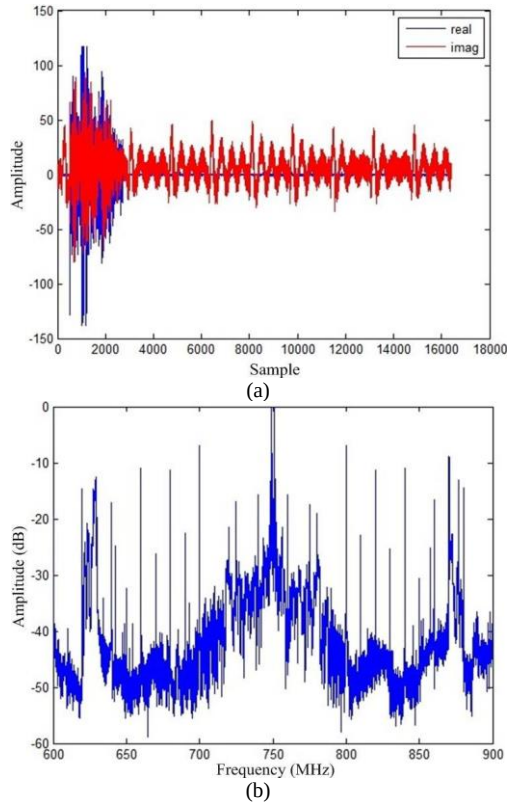

Figure 4. Bistatic scattered data of the illuminated scene. (a) bistatic scattered data from one transmitted radar pulse, including the real (blue line) and imaginary component (red line); (b) sum of the frequency spectrum of the bistatic scattered data from 100 transmitted radar pulses.

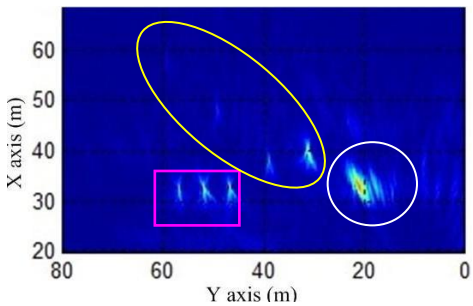

Figure 5. LF UWB OS-BSAR image obtained by the FFBP method.

V. Conclusion

Vehicle experiment the LF UWB OS-BSAR system operating in P-band was performed using a LF UWB SAR system as the vehicle-based transmitter and the other LF UWB radar system as the ground-based receiver. After the processing of the acquired bistatic data, the high quality BSAR image was obtained, which validates the imaging property of the LF UWB OS-BSAR system. A more extensive of the LF UWB BSAR experiments with different operation modes will be carried out in the future.

Acknowledgment

This work was supported in part by the National Natural Science Foundation of China under Grants 61571447, in part by the Scientific Research Project of Education Department of Hunan under Grant 16C1233, and in part by the Domain Foundation of Equipment Advance Research of 13th Five-year Plan under Grants 6140410301 and 6140410304. Daoxiang An is the corresponding author. Xiaotao Huang and Zhimin Zhou are also the authors of this paper, who are also with the College of Electronic Science, National University of Defense Technology (NUDT). I would like to thank them for their competent and helpful suggestions to improve this paper.

References

[1] W. Carrara, R. Goodman, and R. Majewski, *Spotlight Synthetic Aperture Radar: Signal Processing Algorithms*, Norwood, MA, USA: Artech House, 1995.

[2] I. G. Cumming and F. H. Wong, *Digital Processing of Synthetic Aperture Radar Data: Algorithm and Implementation*, Norwood, MA, USA: Artech House, 2005.

[3] D. X. An, X. T. Huang, T. Jin, and Z. M. Zhou, "Extended two-Step focusing approach for squinted spotlight SAR imaging," *IEEE Trans. Geosci. Remote Sens*., vol. 50, no. 7, pp. 2889-2900, July 2012.

[4] H. T. Xie, D. X. An, X. T. Huang, and Z. M. Zhou, "Efficient raw signal generation based on equivalent scatterer and subaperture processing for SAR with arbitrary motion," *Radioengineering*, vol. 23, no. 4, pp. 1169-1178, December 2014.

[5] H. T. Xie, D. X. An, X. T. Huang, and Z. M. Zhou, "Spatial resolution analysis of low frequency ultrawidebeam-ultrawideband synthetic aperture radar based on wavenumber domain support of echo data," *J. Appl. Remote Sens.*, vol. 095033, no. 10, pp. 1-20, January 2016.

[6] H. T. Xie, *et al.*, "Efficient time-domain imaging processing for one-stationary bistatic forward-looking SAR including motion errors," *Sensors*, vol. 16, no. 11, pp. 1-27, November 2016.

[7] I. Walterscheid, *et al.*, "Bistatic SAR experiments with PAMIR and TerraSAR-X-Setup, processing, and image results," *IEEE Trans. Geosci. Remote Sens.*, vol. 48, no. 8, pp. 3268-3279, August 2010.

[8] M. R. Cassola, *et al.*, "First bistatic spaceborne SAR experiments with TanDEM-X," *IEEE Geosci. Remote Sens. Lett.*, vol. 9, no. 1, pp. 33-37, January 2012.

[9] R. Baqué, *et al.*, "LORAMbis A bistatic VHF/UHF SAR experiment for FOPEN," in *Proc. IEEE Radar Conf.*, Washington, USA, 2010, pp. 832-837.

[10] H. T. Xie, D. X. An, X. T. Huang, and Z. M. Zhou, "Fast time-domain imaging in elliptical polar coordinate for general bistatic VHF/UHF ultra-wideband SAR with arbitrary motion," *IEEE J. Sel. Topics Appl. Earth Observ.*, vol. 8, no. 2, pp. 879-895, February 2015.

[11] H. T. Xie, D. X. An, X. T. Huang, and Z. M. Zhou, "Efficient raw signal generation based on equivalent scatterer and subaperture processing for one-stationary bistatic SAR including motion

errors," *IEEE Trans. Geosci. Remote Sens.*, vol. 54, no. 6, pp. 3360-3377, June 2016.
[12] H. T. Xie, D. X. An, X. T. Huang, and Z. M. Zhou, "Research on spatial resolution of one-stationary bistatic ultrahigh frequency ultrawidebeam-ultrawideband SAR based on scattering target wavenumber domain support," *IEEE J. Sel. Topics Appl. Earth Observ.*, vol. 8, no. 4, pp. 1782-1798, April 2015.
[13] M. E. Davis, *Foliage Penetration Radar: Detection and Characterization of Objects Under Trees*, New York, NY, USA: Scitech Pub. Inc., 2011.
[14] D. X. An, Y. H. Li, X. T. Huang, X. Y. Li, and Z. M. Zhou, "Performance evaluation of frequency-domain algorithms for chirped low frequency UWB SAR data processing," *IEEE J. Sel. Topics Appl. Earth Observ.*, vol. 7, no. 2, pp. 678-690, February 2014.
[15] H. T. Xie, *et al.*, "Fast factorized backprojection algorithm for one-stationary bistatic spotlight circular SAR image formation," *IEEE J. Sel. Topics Appl. Earth Observ.*, vol. 10, no. 4, pp. 1494 - 1510, April 2017.
[16] L. M. H. Ulander, A. Gustavsson, T. Jonsson, R. Ragnarsson, and G. Stenström, "Development of CARINA bistatic VHF-band SAR," in *Proc. Int. Radar Conf.*, France, 2014, pp. 601-606.
[17] L. M. H. Ulander, P. O. Frölind, A. Gustavsson, R. Ragnarsson, and G. Stenström, "VHF/UHF bistatic and passive SAR ground imaging," in *Proc. IEEE Int. Radar Conf.*, Arlington, VA, USA, 2015, pp. 669-673.
[18] H. T. Xie, D. X. An, X. T. Huang, X. Y. Li, and Z. M. Zhou, "Fast factorised backprojection algorithm in elliptical polar coordinate for one-stationary bistatic very high frequency/ultrahigh frequency ultra wideband synthetic aperture radar with arbitrary motion," *IET Radar Sonar Navig.*, vol. 8, no. 8, pp. 946-956, October 2014.
[19] D. X. An, L. P. Chen, and X. T. Huang, "Modified nonlinear chirp scaling algorithm for one-stationary bistatic low frequency ultrawideband synthetic aperture radar imaging," *J. Appl. Remote Sens.*, vol. 9, no. 1, pp. 1-11, January 2015.
[20] Z. Dong, D. Liang, and X. Huang, "A RFI suppression algorithm based channel equalization for the VHF/UHF UWB SAR," *J. Elec. Inf. Tech.*, vol. 30, no. 3, pp. 550-553, 2008.

Hongtu Xie was born in Hunan, China, in 1986. He was received the B.S. degree in electronic information engineering from the Hunan University, Changsha, China, in 2008, and received the M.S. degree in electronic science and technology and Ph.D. degree in information and communication engineering from National University of Defense Technology (NUDT), Changsha, China, in 2010 and 2015, respectively.

He is currently a Lecturer with the Shanghai Jiao Tong University (SJTU), with the Hunan University, with the Air Force Early Warning Academy, and also with the NUDT. His research interests include the ultrawideband synthetic aperture radar (SAR), low frequency SAR, bistatic SAR, circular SAR, and SAR-GMTI.

Shaoying Shi was born in Hunan, China, in 1975. He was received the B.S. and M.S. degrees in instrument science and technology from the NUDT, Changsha, China, in 1998 and 2004, respectively, and received the Ph.D. degree in information and communication engineering from the China Academy of Electronics and Information Technology, Beijing, China, in 2016.

He is currently an Associate Professor with the Air Force Early Warning Academy. His research interests include communication and information system and radar signal processing.

Junfa Mao was born in Hunan, China, in 1965. He was received the B.S. degree in radiation physics from the NUDT, Changsha, China, in 1985, the M.S. degree in experimental nuclear physics from the Shanghai Institute of Nuclear Research, Shanghai, China, in 1988, and the Ph.D. degree in electronic engineering from the SJTU, Shanghai, in 1992. He was a Visiting Scholar at the Chinese University of Hong Kong, Hong Kong, from 1994 to 1995, and a postdoctoral researcher at the University of California, Berkeley, from 1995 to 1996.
He is currently a Full Professor with the SJTU. His research interests include the interconnect and package problem of integrated circuits and systems, analysis and design of microwave circuits.

Daoxiang An was born in Jilin, China, in 1982. He was received the B.S., M.S. and Ph.D. degrees in information and communication engineering from the NUDT, Changsha, China, in 2004, 2006 and 2011. He is currently a Lecturer with the NUDT. His research interests include ultrawideband SAR, circular SAR, SAR interferometry, and SAR-GMTI.

Fuhai Li was born in Guangxi, China, in 1964. He was received the B.S. degree in instrument and the M.S. degrees in theory of electrical from the Hunan University, Changsha, China, in 1986 and 1988, respectively. He is currently a Full Professor with the Hunan University, and the Associate President of School of Electrical and Information Engineering, Hunan University. His research interests include the embedded system application and electronic technology application.